



Effect of Gas Pressure on Polarization of SOFC Cathode Prepared by Plasma Spray

Cheng-Xin Li, Zhun-Zhun Wang, Shuai Liu, and Chang-Jiu Li

(Submitted September 30, 2012; in revised form November 29, 2012)

A cermet-supported tubular SOFC was fabricated using thermal spray. The cell performance was investigated at temperatures from 750 to 900 °C and pressures from 0.1 to 0.5 MPa to examine the effect of operating gas pressure on the cell performance. The influence of gas pressure on the cathodic polarization was studied through the electrochemical impedance approach to examine the controlling electrochemical processes during cell operation. Results show that increasing the operating gas pressure improves the power output performance significantly. When the gas pressure is increased from 0.1 to 0.3 MPa, the maximum power density is increased by a factor of 32% at a temperature of 800 °C. The cathode polarization decreases significantly with the increase of the gas pressure. The electrochemical analysis shows that the main control processes of the cathode reaction are the oxygen species transfer at the three-phase boundary and oxygen diffusion on the surface or in the bulk of the cathode, which are enhanced with increasing gas pressure.

Keywords atmospheric plasma spray, cathode, gas pressure, solid oxide fuel cell (SOFC)

1. Introduction

With the background of global warming and rising oil price, the development of low carbon economy has become a hot topic, which is the fundamental way to deal with climate change and environmental crisis. Solid oxide fuel cell (SOFC) is one of the effective power generation technologies and it has many advantages such as high theoretic efficiency; the possibility to use natural gas, biogas, and methane as fuel; noiseless operation; no need to use noble metals as catalysts; and low emissions (Ref 1, 2).

Besides increasing the operating temperature which significantly increases the output performance, increasing the operating pressure can also improve the output performance of SOFC. Singhal (Ref 3) reported that when the operating pressure changed from 0.1 to 0.5 MPa, the maximum output power of the tubular cell with cathode support increased by 9%, and the maximum output power only increased by 6% as the gas pressure increased from 0.5 to 1.5 MPa at the temperature of 1000 °C. Zhou et al. (Ref 4) also reported that when the pressure increased

from 0.1 to 0.6 MPa, the maximum output power density of the tubular cell with anode support increased from 267 to 306 mW/cm² at 800 °C.

On the other hand, a power system with high efficiency of fuel utilization can be obtained by cogeneration of SOFC with gas turbine and steam turbine. The pressurized SOFC operated at 0.3–0.5 MPa can be combined with a gas turbine by feeding exhausted gases into combustors, and such a hybrid power system is expected to reach efficiencies over 70% (Ref 5). Lim et al. reported that the maximum output power of the cell stack increased from 4.3 kW at ambient atmospheric pressure to 5.1 kW in a pressure of 0.35 MPa, with an increase of 18.6% at the temperature of 800 °C (Ref 6). Siemens Westinghouse Power Corporation has developed a 200 kW class pressurized SOFC-GT hybrid power generation demonstration system, and the compressed gas went through SOFC to promote gas turbine to generate power. Its efficiency of electricity generation was 52%, while the power generation efficiency of such systems at ambient pressure is only 46% (Ref 5). Therefore, it is clear that the increasing operation gas pressure leads to the improvement of power output performance of SOFC.

The cathode polarization becomes the main cause of the power losses in SOFC with the decrease of the electrolyte thickness and the optimization of the anode structure (Ref 7, 8). The output performance of SOFC is often limited by the oxygen reduction processes at the cathode, especially at low temperatures (Ref 9–11). High operating pressure can promote the gas diffusion, accelerate the electrode reaction, and then reduce the losses at the electrode (Ref 4, 12). However, few investigations were performed to examine how the pressure influences fundamental electrochemical processes of electrode reactions.

In this study, a cermet-supported tubular SOFC has been fabricated using flame spray and plasma spray, which

Cheng-Xin Li, Zhun-Zhun Wang, Shuai Liu, and Chang-Jiu Li, State Key Laboratory for Mechanical Behavior of Materials, School of Materials Science and Engineering, Xi'an Jiaotong University, Xi'an 710049, Shaanxi People's Republic of China. Contact e-mail: licx@mail.xjtu.edu.cn., licj@mail.xjtu.edu.cn

are regarded as cost-effective methods to reduce the cost of commercial SOFC. The tubular cell performance was investigated at temperatures from 750 to 900 °C and pressures from 0.1 to 0.5 MPa to examine the effect of operating gas pressure on the performance of SOFC. Moreover, the influence of gas pressure on the cathodic polarization was studied through the electrochemical impedance approach.

2. Experimental

2.1 Fabrication of Cell

A free-standing NiCr-Al₂O₃ tube, which is about 450 mm long with an inner diameter of 16 mm, was fabricated by oxygen-acetylene flame spraying (QT-E2000-7/H, SHANGHAI) using a powder blend of NiCr, Al₂O₃, and polyester. Anode, electrolyte, and cathode were successively deposited on the support by atmospheric plasma spray (APS, GDP-80, 80 kW class, JIUJIANG). The agglomerated NiO/YSZ powder was used as anode material. Before the spraying of the cathode, the as-sprayed electrolyte was densified with nanosized YSZ particle suspension in nitrates' solution. The materials' selections and the preparation methods and parameters for different functional layers are shown in Table 1.

2.2 Characterization

The output performance was measured at different temperatures from 700 to 900 °C and pressures from 0.1 to 0.5 MPa, respectively. Hydrogen and oxygen were supplied to the anode side and the cathode side, respectively. An electrochemical workstation (Thales IM6ex, Zahner® Elektrik, Germany) was used for the electrochemical impedance measurement. The tests were performed in a frequency range from 0.1 to 10⁵ Hz with an amplitude of the AC signal of 10 mV at the equilibrium potential. A three-electrode setup was used to measure the polarization (Ref 13). During the measurement, in order to avoid the interactions between the work electrode and reference electrode, the distance between them should be longer than three times that of the electrolyte thickness (Ref 14, 15). Pt wires were used as the leads of the three electrodes. Before the test, the single cells were treated in protective atmosphere at 800 °C for 2 h.

The cross section morphology of the tubular single cell was characterized by scanning electron microscopy (SEM) (VEGA II-XMU, TSCAN, Brno, Czech Republic).

3. Results and Discussion

3.1 Microstructure of the Single Cell

Figure 1 shows the cross section morphology of the thermally sprayed tubular single cell. As shown in Fig. 1(a), in addition to the porous cermet support, it contains anode, electrolyte, and cathode. The cathode and anode are well bonded with electrolyte, which contributes to a steady performance of the cell in the long run. Electrolyte prepared by thermal spray is relatively dense after the densification process (Ref 16, 17) and is sufficient to isolate the gas of the cathode from that of the anode. The interconnecting of the pores in the anode can be achieved by both the inherent pores in the lamellae and the additional pores produced after reduction of NiO to Ni metal. Figure 1(b) shows the cross-sectional microstructure of the plasma-sprayed cathode. Pores in the deposit consist of relatively large voids and small two-dimensional voids such as the interlamellar non-bonded interfaces and microcracks in individual lamellae. Pores are therefore interconnected through microcracks in individual splats in the cathode (Ref 18), which permit the passage of gas through the cathode. The porosity of the plasma-sprayed LSM cathode with a thickness less than 50 μm is enough to diffuse reacting gas to the triple-phase boundary (TPB) zone (Ref 16, 19).

3.2 Effect of Pressure on the Output Performance

Figure 2 shows the typical current-voltage characteristic and the corresponding power densities at the temperature of 900 °C for the tubular single cell. The open circuit voltage (OCV) of the cell is comparable to the theoretic value, which implies that dense electrolyte was obtained by post-spray densification of plasma-sprayed YSZ. It can be seen that the OCV increases with the increase of operating pressure, which is consistent with the theoretic calculation (Ref 20). The fact that the OCV continuously increases with the pressure increase also implies that the thermally sprayed tubular cell is stable at the tested pressure range.

Figure 3 shows the effect of operating temperatures and pressures on the maximum output power density at different pressures. It can be found that with the increase of operating pressure, the maximum power density increased. The maximum power density at 900 °C was increased by the factors of 22.0 and 32.8% when the operating pressure was changed from 0.1 to 0.2 MPa and from 0.1 to 0.3 MPa, respectively. The effect of pressure on the performance at different operating temperatures is similar to that at 900 °C. When the operating pressure

Table 1 Nominal compositions and processing methods of SOFC components

| Components | Composition | Processing method | Spray power, kW | Spray distance, mm | Thickness, μm |
|----------------|---|-------------------|-----------------|--------------------|---------------|
| Cermet support | Ni50Cr50-Al ₂ O ₃ | FS | ... | 90 | 1000 |
| Anode | NiO-YSZ | APS | 30 | 100 | 20 |
| Electrolyte | YSZ | APS | 42 | 75 | 110 |
| Cathode | LSM | APS | 30 | 100 | 20 |

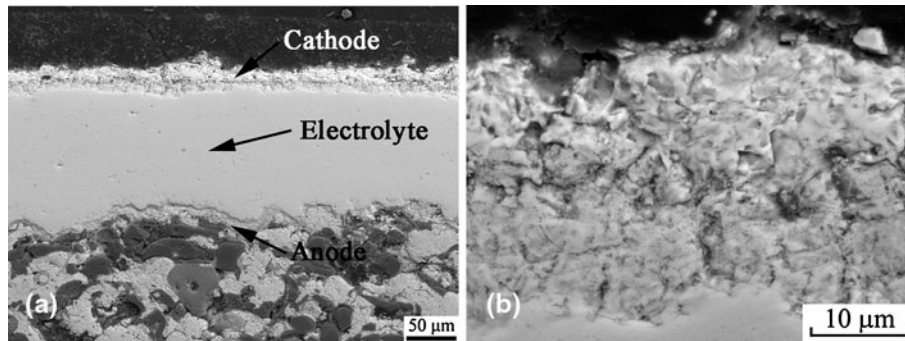


Fig. 1 Cross section morphology of the thermal sprayed tubular single cell. (a) Overall morphology of the cell and (b) cathode morphology

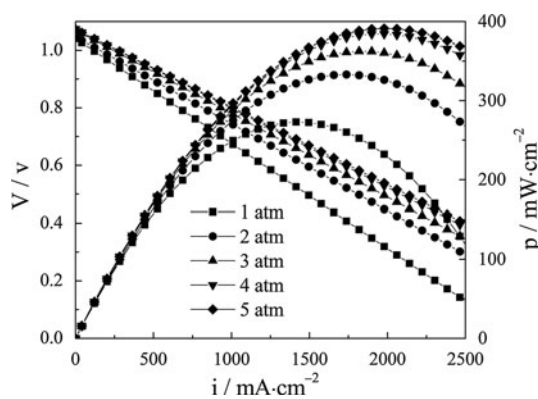


Fig. 2 Output performance of the tubular cell at 900 °C under different pressures

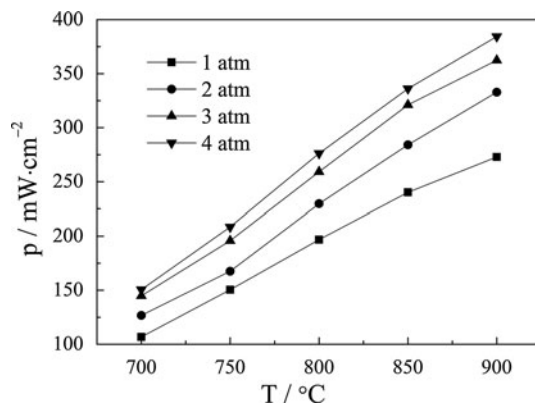


Fig. 3 The maximum power density at different temperatures and pressures

increased from 0.1 to 0.3 MPa, the maximum power density was increased about 31.7% at the temperature of 800 °C as shown in Fig. 3. When the operating pressure became higher than 0.3 MPa, the increasing rate becomes less than that at a lower pressure range.

3.3 Effect of Pressure on Polarization

Figure 4 shows Nyquist diagrams of pressured cells at the temperatures from 750 to 900 °C and the operating pressures from 0.1 to 0.5 MPa. As shown in Fig. 4, each Nyquist plot consists of two depressed arcs. Intercepts of the Z_{re} axis with each Nyquist plot at high frequency represent the Ohmic polarization of the system R_s , while the area-specific polarization R_p is determined by the difference between the intercepts at high and low frequencies. It was obvious that R_s only depends on operating temperature and R_p depends both on temperature and pressure. Therefore, both R_s and R_p decreased with increasing temperature at the same operating pressure. When the test temperature was 750 °C and operating pressure was 0.1 MPa, R_s and R_p were 2.35 and 1.49 $\Omega\cdot\text{cm}^2$, respectively, while at 900 °C and 0.1 MPa, they were reduced to 2.19 and 0.82 $\Omega\cdot\text{cm}^2$, respectively. Moreover, R_p decreased with the operating pressure at different temperatures. At 900 °C, R_p decreased from 0.82 to 0.35 $\Omega\cdot\text{cm}^2$ when the operating pressure was increased from 0.1 to 0.5 MPa.

When the operating pressure increases, the oxygen pressure of the cathode side will change. However, the oxygen pressure at the anode side changes little. This is because oxygen partial pressure of the anode side is only related to the ratio of $P_{\text{H}_2\text{O}}$ to P_{H_2} , while that of the cathode side is proportional to the overall gas pressure (Ref 21). Moreover, the Ohmic polarization is not influenced by the gas pressure. The changes of polarization measured by the three-electrode setup at different pressures represent the changes of cathode polarization.

Jorgensen and Mogensen (Ref 22) suggested that there are at least five processes which affect the impedance. They are presented from high to low frequency below. Two processes are related to the transport of oxide ions and/or oxygen intermediates within the electrode structure and at the electrode/electrolyte interface, and the two processes correspond to the highest frequency range and are often difficult to separate. Their contribution to the impedance is usually small or negligible. The third process reflects competitive elementary steps in the oxygen reduction reaction. This process depends on the TPB length and is often found to be the major contributor to the impedance. It is assumed that this process may be

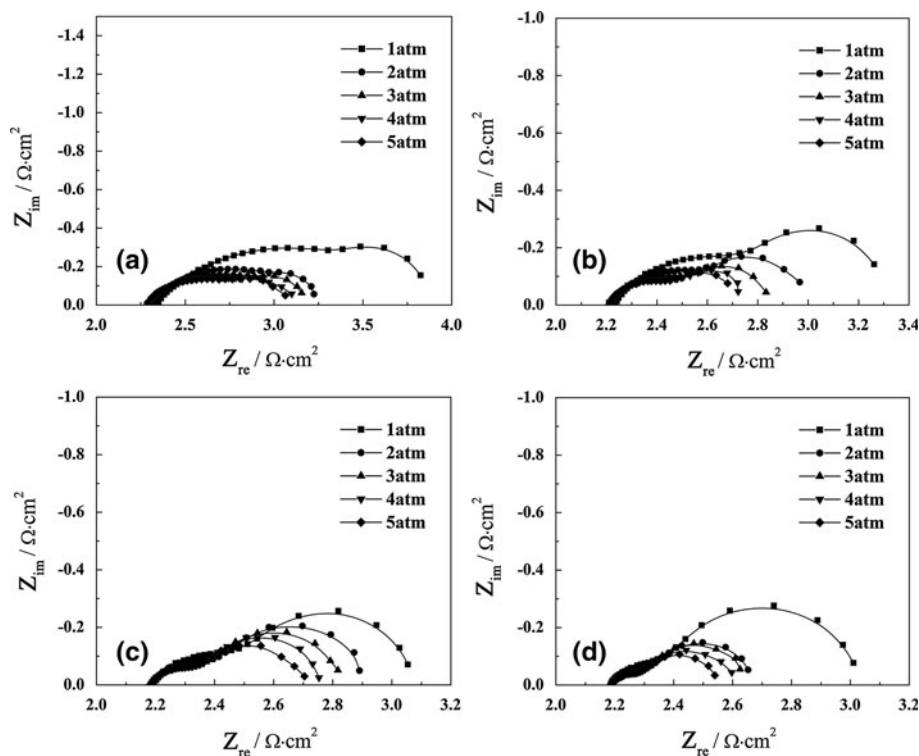


Fig. 4 Nyquist diagrams of pressured cathode at different pressures and temperatures. (a) 750 °C, (b) 800 °C, (c) 850 °C, and (d) 900 °C

dominated by dissociative adsorption, transfer of species at the TPB, or surface diffusion depending on the circumstances. Another main contributor to the impedance is a process corresponding to oxygen diffusion in the porous cathode structure and in a stagnant gas layer above the electrode structure. The last process corresponds to an inductive arc at very low frequencies. Not all the arcs and processes can be identified in the acquired impedance spectra. However, according to the different frequency ranges of the arcs, the control processes of the electrode reaction can be determined.

There were only two depressed arcs obtained in this study. It was simulated by the commercial software Zplot/Zview (Solatron Instruments Ltd.) to further investigate the control processes of the cathode reaction at different pressures. The equivalent circuit is shown in Fig. 5, where L1 represents the inductor, R_s represents the Ohmic resistance, R1 and R2 are the polarization resistances, and CPE1 and CPE2 are constant phase elements. From the phase angle plots tested at 900 °C shown in Fig. 6, it is clear that the impedance characteristics are mainly determined by two different processes, which corresponds to the two partially overlapping depressed arcs in the Nyquist plots. Kournoutis et al. (Ref 23) also reported that overlapping of different arcs is more pronounced at lower temperatures. On the other hand, the inductance was taken into account in the simulation to exclude its influence on the simulation of R1 and R2. However, the inductance which should appear in the fourth quadrant cannot be seen on the Nyquist plots because the Nyquist plots were drawn with a vertical coordinate starting from



Fig. 5 The equivalent circuit of the Nyquist plots

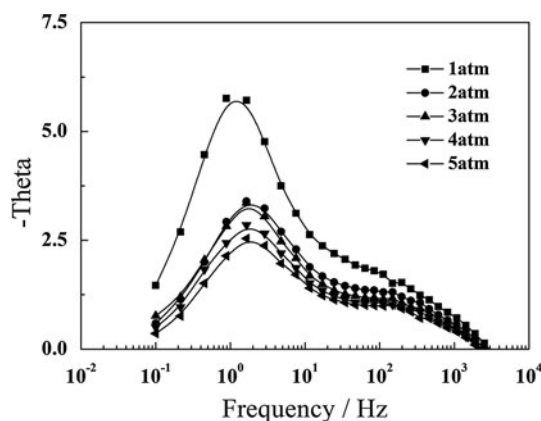


Fig. 6 Bode plots acquired at 900 °C

zero in Fig. 4. Based on the equivalent circuit in Fig. 5, the simulation by fitting the Nyquist plots at 900 °C yielded the values shown in Table 2. It can be found that the polarization resistances R1 and R2 decreased with the increasing gas pressure, while the Ohmic polarization was not affected by the pressure.

Table 2 Fitting data of the Nyquist plots at 900 °C

| | 0.1 MPa | 0.2 MPa | 0.3 MPa | 0.4 MPa | 0.5 MPa |
|---------------------------|---------|---------|---------|---------|---------|
| $R_s, \Omega\text{-cm}^2$ | 2.159 | 2.168 | 2.170 | 2.176 | 2.176 |
| $R_1, \Omega\text{-cm}^2$ | 0.288 | 0.181 | 0.155 | 0.133 | 0.124 |
| $R_2, \Omega\text{-cm}^2$ | 0.591 | 0.328 | 0.322 | 0.300 | 0.252 |

In Fig. 4, it can be found that the frequency range of the high frequency arc is about 200-3000 Hz, while that of the low frequency arc is about 0.1-200 Hz. According to the frequency ranges of each depressing arc and their responses to the changes of gas pressure, corresponding to the reports of Jorgensen and Mogensen (Ref 22), it can be confirmed that the process of the high frequency arc corresponds to the transfer of oxygen species at the TPB, while that of the low frequency arc corresponds to oxygen diffusion in the porous cathode structure and in a stagnant gas layer above the electrode structure.

The dependence of the cathode polarization on oxygen pressure can be expressed as follows (Ref 24):

$$R_{el} = k(P_{O_2})^{-n}$$

where R_{el} represents the cathode polarization resistance / $\Omega\text{-cm}^2$, k is the speed constant, P_{O_2} is the oxygen pressure / Pa, and n is the index of oxygen pressure. Takeda et al. (Ref 25) reported that the n value of 0.5 corresponds to the process controlled by oxygen atom concentration and the n value of 1 corresponds to the process controlled by oxygen molecule concentration. In this study, the n value of the high frequency arc is 0.44-0.52 and that of the low frequency arc is 0.47-0.48. Thus, the two control processes of the cathode reaction are both related to atomic oxygen concentration.

The CPE as shown in Fig. 5 can also be calculated from the software Zplot/Zview. With the increase of gas pressure from 0.1 to 0.5 MPa, the capacitance that corresponds to the low frequency arc increased from 0.32 to 0.53 F/cm^2 . As shown in Fig. 6, the frequency corresponding to the highest point of the low frequency arc basically changes little with the change of gas pressure, remaining 1.5 Hz. With such a low frequency and a high value of capacitance, this semicircle is usually assigned to processes such as gas diffusion or dissociative diffusion related to oxygen depletion (Ref 26).

Based on the previous results, the cathode reaction in this study is controlled by two processes. The low frequency process is the diffusion behavior of oxygen in the porous cathode structure and in a stagnant gas layer above the electrode structure, and the high frequency process is the transfer of oxygen species at the TPB.

With the increase of gas pressure, the concentration of reacting gas increases, which benefits oxygen adsorption and dissociation on the cathode surface and thus atomic oxygen diffusion on the surface or in the bulk of cathode. Meanwhile, oxygen species transfer at the TPB would be promoted. The increase of gas pressure, through its effects on the two control processes of the cell reaction, reduces the polarization loss and thus promotes the cell output performance.

4. Conclusions

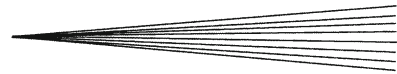
A cermet-supported tubular SOFC was fabricated using thermal spray. The effect of operating pressure on cell performance was investigated at temperatures from 750 to 900 °C and pressures from 0.1 to 0.5 MPa. The results showed that with increasing operating pressure, the cell performance would be significantly improved, especially at low operating pressures. When the operating pressure increased from 0.1 to 0.3 MPa, the maximum power density was increased about 31.7% at the temperature of 800 °C. The cathode polarization decreased by about 38.9% when the operating pressure increased from 0.1 to 0.3 MPa at 800 °C. The main control processes of the cathode reaction were the oxygen species transfer at the TPB and oxygen diffusion on the surface or in the bulk of the cathode.

Acknowledgments

The present study was financially supported by the National Basic Research Program of China (Grant No. 2012CB625104) and the National Nature Science Foundation of China (Grant No. 51072161).

References

- N.H. Menzler, F. Tietz, S. Uhlenbruck, H.P. Buchkremer, and D. Stover, Materials and Manufacturing Technologies for Solid Oxide Fuel Cells, *J. Mater. Sci.*, 2010, **45**(12), p 3109-3135
- J.W. Wu and X.B. Liu, Recent Development of SOFC Metallic Interconnect, *J. Mater. Sci. Technol.*, 2010, **26**(4), p 293-305
- S.C. Singhal, Advances in Solid Fuel Cell Technology, *Solid State Ionics*, 2000, **135**, p 305-313
- L. Zhou, M.J. Cheng, B.L. Yi, Y.L. Dong, Y. Cong, and W.S. Yang, Performance of an Anode-Supported Tubular Solid Oxide Fuel Cell Under Pressurized Conditions, *Electrochim. Acta*, 2008, **53**, p 5195-5198
- M.C. Williams, J.P. Strakey, and S.C. Subhash, US Distributed Generation Fuel Cell Program, *J. Power Sources*, 2004, **131**(1-2), p 79-85
- T.H. Lim, R.H. Song, D.R. Shin, J.I. Yang, H. Jung, I.C. Vinke, and S.S. Yang, Operating Characteristics of a 5 kW Class Anode-Supported Planar SOFC Stack for a Fuel Cell/Gas Turbine Hybrid System, *Int. J. Hydrogen Energy*, 2008, **33**(3), p 1076-1083
- C.-J. Li, C.-X. Li, Y.-Z. Xing, M. Gao, and G.-J. Yang, Influence of YSZ Electrolyte Thickness on the Characteristics of Plasma-Sprayed Cermet Supported Tubular SOFC, *Solid State Ionics*, 2006, **177**, p 2065-2069
- H. Moon, S.D. Kim, E.W. Park, S.H. Hyun, and H.S. Kim, Characteristics of SOFC Single Cells with Anode Active Layer via Tape Casting and Co-firing, *Int. J. Hydrogen Energy*, 2008, **33**(11), p 2826-2833
- M. Ostergaard, C. Clausen, C. Bagger, and M. Mogensen, Manganese-Zirconia Composite Cathodes for SOFC—Influence of



- Structure and Composition, *Electrochim. Acta*, 1995, **40**(12), p 1971-1981
10. J. VanHerle, A.J. McEvoy, and K.R. Thampi, A Study on the $\text{La}_{1-x}\text{Sr}_x\text{MnO}_3$ Oxygen Cathode, *Electrochim. Acta*, 1996, **41**(9), p 1447-1454
 11. C.W. Tanner, K.Z. Fung, and A.V. Virkar, The Effect of Porous Composite Electrode Structure on Solid Oxide Fuel Cell Performance. 1. Theoretical Analysis, *J. Electrochem. Soc.*, 1997, **144**(1), p 21-30
 12. J. Larminie and A. Dicks, *Fuel Cell Systems Explained*, SAE International and John Wiley & Sons, Ltd., New York, 2003, p 40
 13. Y.J. Leng, S.H. Chan, K.A. Khor, and S.P. Jiang, Performance Evaluation of Anode-Supported Solid Oxide Fuel Cells with Thin Film YSZ Electrolyte, *Int. J. Hydrogen Energy*, 2004, **29**(10), p 1025-1033
 14. S.B. Adler, B.T. Henderson, M.A. Wilson, and D.M. Taylor, Reference Electrode Placement and Seals in Electrochemical Oxygen Generators, *Solid State Ionics*, 2000, **134**, p 35-42
 15. J. Winkler, P.V. Hendriksen, N. Bonanos, and M. Mogensen, Geometric Requirements of Solid Electrolyte Cells with a Reference Electrode, *J. Electrochem. Soc.*, 1998, **145**(4), p 1184-1192
 16. C.-X. Li, C.-J. Li, and G.-J. Yang, Development of a $\text{Ni}/\text{Al}_2\text{O}_3$ Cermet-Supported Tubular Solid Oxide Fuel Cell Assembled with Different Functional Layers by Atmospheric Plasma-Spraying, *J. Therm. Spray Technol.*, 2009, **18**(1), p 83-89
 17. X.-J. Ning, C.-X. Li, C.-J. Li, and G.-J. Yang, Modification of Microstructure and Electrical Conductivity of Plasma-Sprayed YSZ Deposit Through Post-Densification Process, *Mater. Sci. Eng. A*, 2006, **428**(1-2), p 98-105
 18. A. Ohmori, C.-J. Li, Y. Arata, K. Inoue, and N. Iwamoto, Dependence of the Connected Porosity in Plasma Sprayed Ceramic Coatings on Structure, *J. Jpn. High Temp. Soc.*, 1990, **16**, p 332-340 (in Japanese)
 19. K. Barthel, S. Rambert, and St. Siegmann, Microstructure and Polarization Resistance of Thermally Sprayed Composite Cathodes for Solid Oxide Fuel Cell Use, *J. Therm. Spray Technol.*, 2000, **9**(3), p 343-347
 20. T. Malkow, Chap. 1, *Modeling Solid Oxide Fuel Cells: Methods, Procedures and Techniques*, R. Bove and S. Ubertini, Ed., Springer, New York, 2008, p 4
 21. A.V. Virkar, K.Z. Fung, and S.C. Singhal, The Effect of Pressure on Solid Oxide Fuel Cell Performance, *Proceedings of the Third International Symposium on Ionic and Mixed Conducting Ceramics*, T.A. Ramanarayanan, W.L. Worrell, H.L. Tuller, A.C. Khandkar, M. Mogensen, and W. Gopel, Ed., Aug 31-Sep 5, 1997 (Paris), Electrochemical Society, 1997, p 113-124
 22. M.J. Jorgensen and M. Mogensen, Impedance of Solid Oxide Fuel Cell LSM/YSZ Composite Cathodes, *J. Electrochem. Soc.*, 2001, **148**(5), p A433-A442
 23. V.Ch. Kournoutis, F. Tietz, and S. Bebelis, AC Impedance Characterisation of a $\text{La}_{0.8}\text{Sr}_{0.2}\text{Co}_{0.2}\text{Fe}_{0.8}\text{O}_{3-\delta}$ Electrode, *Fuel Cells*, 2009, **9**(6), p 852-860
 24. E.C. Thomsen, G.W. Coffey, L.R. Pederson, and O.A. Marina, Performance of Lanthanum Strontium Manganite Electrodes at High Pressure, *J. Power Sources*, 2009, **191**(2), p 217-224
 25. Y. Takeda, R. Kanno, M. Noda, Y. Tomida, and O. Yamamoto, Cathodic Polarization Phenomena of Perovskite Oxide Electrodes with Stabilized Zirconia, *J. Electrochem. Soc.*, 1987, **134**(11), p 2656-2661
 26. B. Morel, R. Roberge, S. Savoie, T.W. Napporn, and M. Meunier, Catalytic Activity and Performance of LSM Cathode Materials in Single Chamber SOFC, *Appl. Catal. A*, 2007, **323**, p 181-187